

1. Report No. FHWA/TX-05/0-4820-1	2. Government Accession No.	3. Recipient's Catalog No.	
4. Title and Subtitle INVESTIGATION OF A NEW GENERATION OF FCC COMPLIANT NDT DEVICES FOR PAVEMENT LAYER INFORMATION COLLECTION: HARDWARE AND ALGORITHMS		5. Report Date Feb. 2006	
		6. Performing Organization Code	
7. Author(s) Richard Liu, Jing Li, Xuemin Chen, Aditya Ekbote, Huichun Xing, and Ying Wang		8. Performing Organization Report No. 0-4820-1	
9. Performing Organization Name and Address Department of Electrical and Computer Engineering University of Houston 4800 Calhoun Rd. Houston, TX 77204-4005		10. Work Unit No.	
		11. Contract or Grant No. 0-4820	
12. Sponsoring Agency Name and Address Texas Department of Transportation Research and Technology Implementation Office P. O. Box 5080 Austin, TX 78763-5080		13. Type of Report and Period Covered Technical Report: September 2003 – August 2005	
		14. Sponsoring Agency Code	
15. Supplementary Notes Project performed in cooperation with the Texas Department of Transportation and the Federal Highway Administration. Project title: Investigation of a New Generation of FCC Compliant NDT Devices for Pavement Layer Information Collection URL: http://tti.tamu.edu/documents/0-4820-1.pdf			
16. Abstract: The Federal Communications Commission (FCC) adopted a new rule on ground penetrating radar (GPR) devices on July 12, 2002, that permits the operation of GPRs and wall imaging systems only below 960 MHz and between 3.1 and 10.6 GHz. To comply with new FCC regulations, a hybrid GPR system is developed which includes the following two individual radars: 1) a pulse GPR radar working in the frequency range from DC to 900 MHz for thick pavement layer and subgrade layer thickness and moisture detection; and 2) a frequency-modulated continuous-wave (FMCW) radar working in the frequency range from 3.1 to 8.5 GHz for measuring thin asphalt layers. The GPR data format is now compatible with Texas Department of Transportation (TxDOT) software, which benefits the information sharing and the implementation of this FCC compliant GPR system. Laboratory tests and field tests have been conducted. The measured results agree with the real cases very well.			
17. Key Words FCC Rules on GPR, FCC-Compliant GPR, Pavement Thickness and Dielectric Constant Measurement, Network Level Layer Information Collection		18. Distribution Statement No restrictions. This document is available to the public through National Technical Information Service, Springfield, Virginia, 22161 http://www.ntis.gov .	
19. Security Classif. (of this report) Unclassified	20. Security Classif. (of this page) Unclassified	21. No. of Pages 44	22. Price

Form DOT F 1700.7 (8-72)

This form was electrically by Elite Federal Forms Inc.

**Investigation of a New Generation of FCC Compliant NDT Devices for
Pavement Layer Information Collection: Hardware and Algorithms**

by

Richard Liu, Jing Li, Xuemin Chen, Aditya Ekbote, Huichun Xing, and Ying Wang

Technical Report 0-4820-1

Project Number: 0-4820

Project Title: Investigation of a New Generation of FCC Compliant NDT Devices for
Pavement Layer Information Collection

Performed in Cooperation with the
Texas Department of Transportation
and the
Federal Highway Administration

by the

Subsurface Sensing Laboratory
Department of Electrical and Computer Engineering
University of Houston

February 2006

DISCLAIMER

The contents of this report reflect the views of the authors, who are responsible for the facts and accuracy of the data presented herein. The contents do not necessarily reflect the official views or policies of the Texas Department of Transportation or the Federal Highway Administration. This report does not constitute a standard, specification or regulation.

University of Houston
4800 Calhoun Rd.
Houston, TX 77204

ACKNOWLEDGMENTS

This project was sponsored by the Texas Department of Transportation and the Federal Highway Administration. The research work was greatly supported by Project Director Brian Michalk; Program Coordinator Ed Oshinski; and Research Engineer Dr. German Claros.

TABLE OF CONTENTS

LIST OF FIGURES	viii
LIST OF TABLES	ix
CHAPTER 1: INTRODUCTION.....	1
CHAPTER 2: HYBRID GPR SYSTEM	3
2.1 LOW FREQUENCY PULSE GPR	3
2.2 FREQUENCY CONTROL FOR THE PULSE GPR	4
2.3 HIGH FREQUENCY GPR.....	11
2.4 FREQUENCY CONTROL FOR FMCW GPR.....	13
2.5 DISTANCE MEASUREMENT INSTRUMENT AND GLOBAL POSITIONING SYSTEM.....	14
CHAPTER 3: IMPROVEMENTS IN ALGORITHMS	17
3.1 CURRENT METHODS FOR DIELECTRIC CONSTANT ESTIMATION.....	17
3.2 NEW METHOD FOR DIELECTRIC CONSTANT ESTIMATION FOR GROUND-COUPLED GPR.....	18
CHAPTER 4: LAB AND FIELD TESTS	23
4.1 LAB TESTS OF FMCW RADAR	23
4.2 LAB TESTS OF PULSE GPR.....	26
4.3 FIELD TESTS	27
CHAPTER 5: CONCLUSIONS AND RECOMMENDATIONS.....	31
5.1 CONCLUSIONS.....	31
5.2 RECOMMENDATIONS.....	31
REFERENCES	33

LIST OF FIGURES

Fig. 2-1 Block diagram of the pulse GPR system.....	4
Fig. 2-2 0.75 ns pulse and its spectrum.....	5
Fig. 2-3 1.5 ns pulse and its spectrum.....	6
Fig. 2-4 3 ns pulse and its spectrum.....	7
Fig. 2-5 3.7 ns pulse and its spectrum.....	8
Fig. 2-6 4.5 ns pulse and its spectrum.....	9
Fig. 2-7 Frequency range of a pulse wave versus pulse time duration	10
Fig. 2-8 Ground-coupled version of the pulse GPR	11
Fig. 2-9 Block diagram of the FMCW radar.....	12
Fig. 2-10 FMCW system used for measuring properties of pavement layers	12
Fig. 2-11 Transmitter's output frequency versus applied tune DC voltage.....	13
Fig. 2-12 DMI and GPS equipment setup.....	14
Fig. 2-13 DMI/GPS setup	15
Fig. 3-1 Typical measured ground-coupled GPR waveform.....	19
Fig. 3-2 Main wave paths for ground-coupled GPR.....	19
Fig. 3-3 Geometry for numerical simulation	20
Fig. 3-4 Simulated waveforms at positions R1, R2, R3, R4, and R5	20
Fig. 3-5 Comparison of simulated time and modeled time.....	21
Fig. 4-1 Asphalt slabs for lab experiment.....	23
Fig. 4-2 Slab size.....	23
Fig. 4-3 Measured signals on 11.5 inch slab by FMCW GPR.....	24
Fig. 4-4 A parking lot asphalt pavement with a thickness around 2.75 inches.....	25
Fig. 4-5 Measured FMCW radar waveform over the parking lot.....	25
Fig. 4-6 Waveforms measured by pulse GPR over the asphalt slab.....	27
Fig. 4-7 Measured over Annex at TTI by ground-coupled GPR	28
Fig. 4-8 Measured result on SH21 in Bryan	29

LIST OF TABLES

Table 4-1 Measured thickness of a parking lot pavement	24
--	----

CHAPTER 1: INTRODUCTION

Ground penetrating radar (GPR) is a useful nondestructive tool for collection of subsurface layer information [1] [2] [3]. The frequency range of 10 MHz to a few GHz has been commonly used for decades in GPR applications [4] [5]. However, the Federal Communications Commission (FCC) adopted a new rule on GPR devices on July 12, 2002, that permits the operation of GPRs and wall imaging systems only below 960 MHz or between 3.1 GHz and 10.6 GHz. As we know, the radar frequency influences both the spatial resolution and the penetrating depth underground. Higher frequencies provide higher spatial resolutions but lower penetrating depths, and the lower frequencies can reach larger penetrating depths but have lower spatial resolutions. Fortunately, GPR could always reach a good compromise between its spatial resolutions and the penetrating depths in detection of pavement layers in the frequency band of 10 MHz to 3.1 GHz, i.e., there always exist some frequency components in this band that can reach the deepest layer of any types of pavements to be measured and are able to distinguish the interfaces between different layers. But the FCC regulation forbids the use of the middle portion of this ideal band for GPR and wall imaging systems. To comply with FCC regulations, we have to search for alternative frequency windows for GPR applications. Hence, the first objective of this project is to develop a hybrid GPR system which includes two individual subsystems: 1) a pulse GPR radar working in the frequency range from direct current (DC) to 900 MHz for thick pavement layers and subgrade layers detection; and 2) a frequency-modulated continuous-wave (FMCW) radar working in the frequency range from 3.1 GHz to 8.5 GHz for measuring thin asphalt layers. The second objective is to verify that the developed hybrid GPR system performs good enough to replace the previous GPR versions that work in the forbidden band. Here, the FMCW technique is adopted for the band above 3.1 GHz because it is of the format of radar whose frequency range can be strictly confined within a range high above DC. For a pulse GPR, its spectrum always covers the range from DC to its upper frequency limit. The upper frequency limit is determined by the time duration of pulse waves. The longer the time duration of a pulse

wave, the more low frequency components will be generated; on the other hand, the narrower the pulse wave is, the more high frequency components can be obtained. In [Chapter 2](#), the structures and the features of these two sub-GPR systems will be explained. [Chapter 3](#) will introduce improvements in algorithms for determining the dielectric constant and thickness of pavements directly from GPR data, and the lab and field test data will be displayed in [Chapter 4](#). Conclusions will be delivered in [Chapter 5](#).

CHAPTER 2: HYBRID GPR SYSTEM

To comply with FCC regulations, GPRs can only work in the two separate frequency bands: DC to 960 MHz and 3.1 GHz to 10 GHz. In this project, two types of GPRs, a low frequency pulse GPR and a high frequency FMCW GPR, are developed to form a hybrid GPR system, ultimately utilizing available frequency resources.

2.1 Low Frequency Pulse GPR

A pulse GPR is constructed of a transmitter for generating a time domain pulse, a wideband receiver to pick up the reflected waves, a control circuit unit for system control, a host computer to operate the system and process and display data, a data acquisition circuit, and two sets of wideband antennas. A detailed block diagram is shown in Fig. 2-1, where the components in the red-dashed-line box form the transmitter, the components in the green-dashed-line box make a receiver, and the clock is shared by both the transmitter and receiver. The working principle of a low frequency pulse GPR can be summarized in this way: when the control unit receives a command from the host computer, it triggers the transmitter to emit a short pulse wave into space via the transmitting antenna; at the same time, the control unit also sends a command to the sampling unit to pick up the incoming reflected signals. The transmitted wave from the transmitting antenna usually propagates in all directions in space, and part of it penetrates into the pavement. When the penetrated wave encounters the subsurface interface, it is reflected back and picked up by the receiving antenna. There is also another part of the transmitted wave propagating directly from the transmitting antenna to the receiving antenna or from the transmitting antenna to the pavement surface and then bouncing up to the receiving antenna, which is called the direct wave. The received direct wave and the subsurface reflected wave are both transferred to the host laptop by sampling unit and data acquisition card. By processing the received signals and finding travel times of reflected waves [6], the thickness, dielectric constant, and moisture content of the pavement can be obtained and displayed.

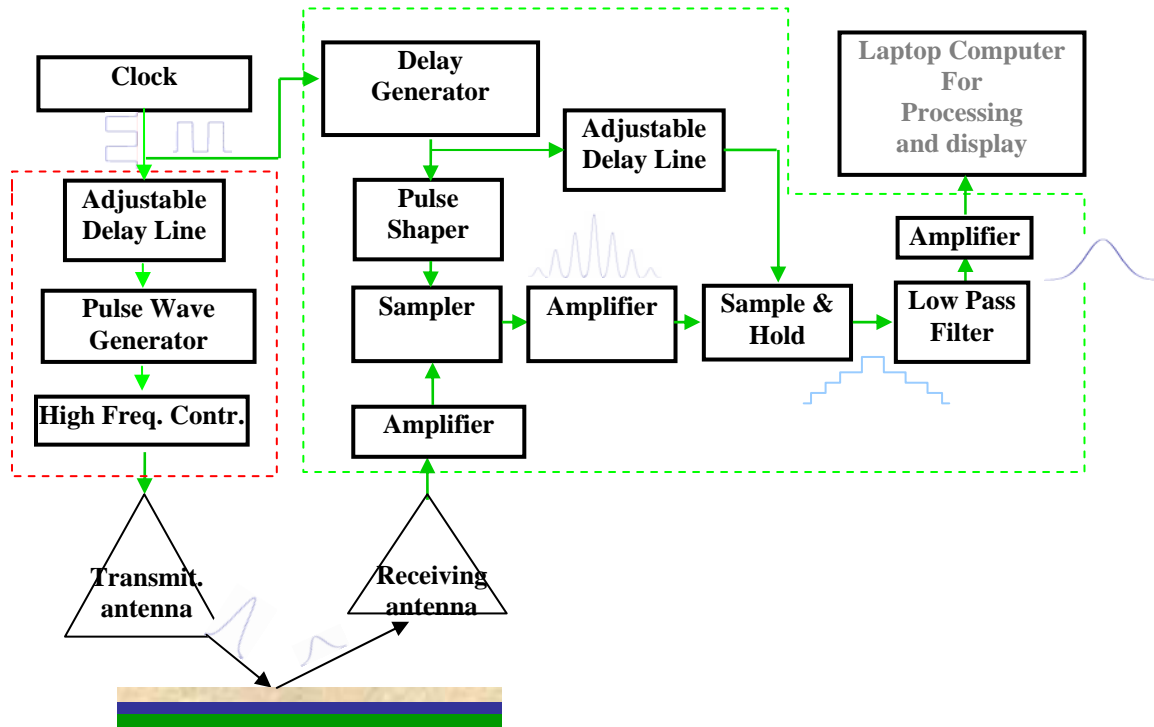
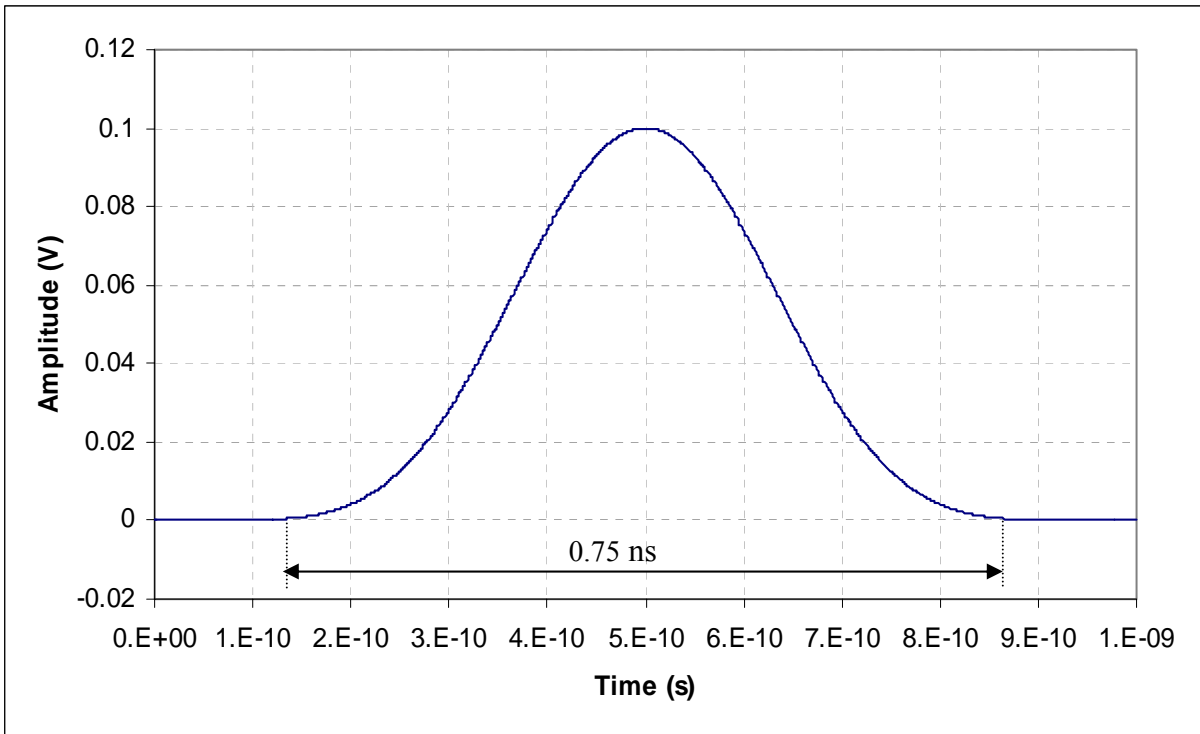


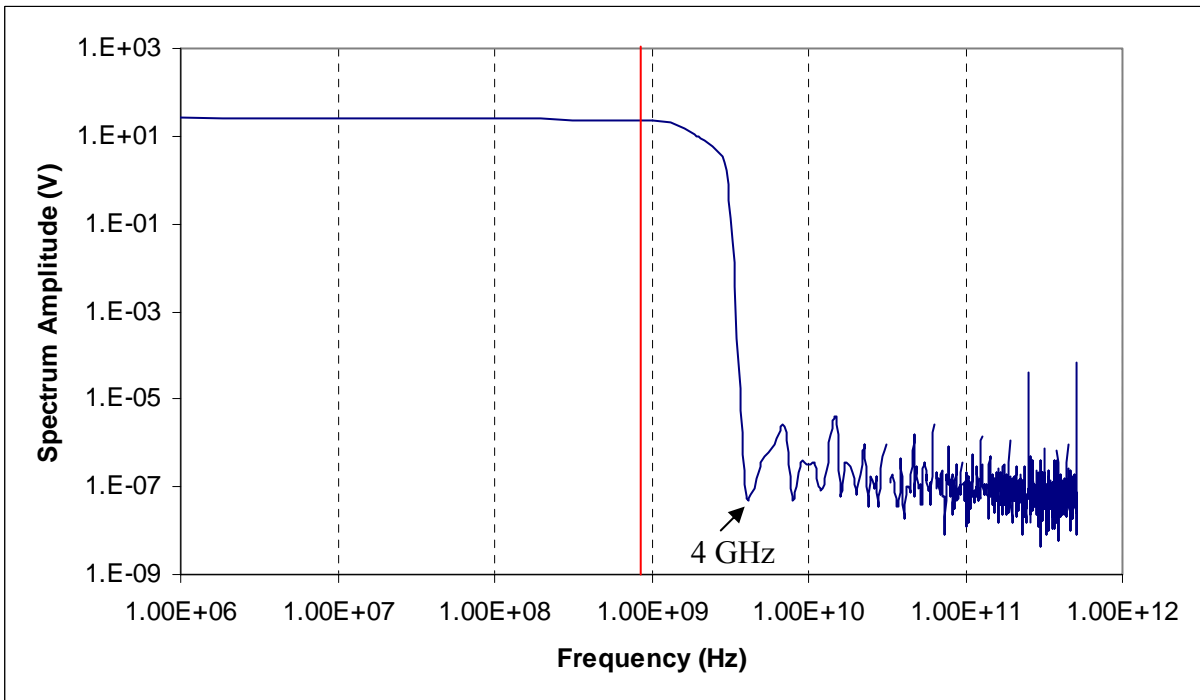
Fig. 2-1 Block diagram of the pulse GPR system

2.2 Frequency Control for the Pulse GPR

To comply with FCC rules, the frequency band of low frequency GPR must be controlled within the range of 960 MHz. Two methodologies are employed in this project to confine the GPR frequency range within DC to 960 MHz. The first one is to adjust the design parameters of transmitters, and the second one is using a low pass filter to remove the components above 960 MHz. In order to quantitatively determine the transmitter parameters, the relationship between the pulse width and its spectrum band is numerically studied, and the results are illustrated in Figs. 2-2 through 2-6. In these figures, (a) is a pulse waveform with amplitude of 0.1 V, and (b) gives its spectrum. From Fig. 2-2 it can be seen that when the width of a Gaussian type pulse is 0.75 ns, its spectrum extends to 4 GHz, covering the whole banned band.

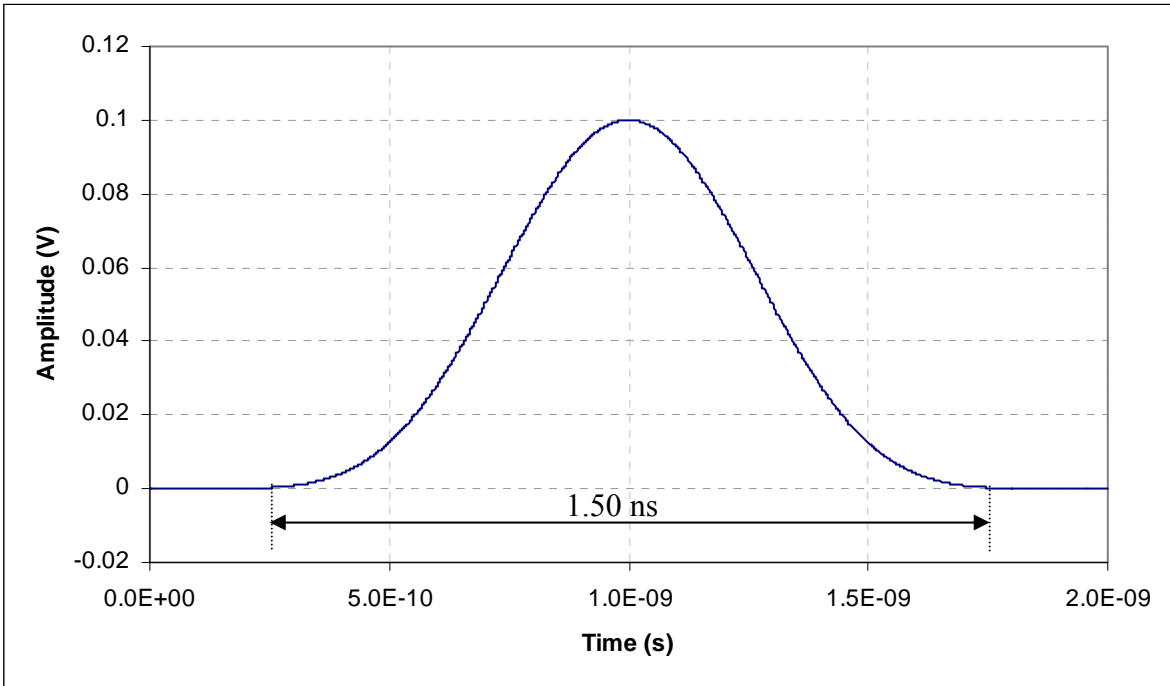


(a) 0.75 ns pulse waveform

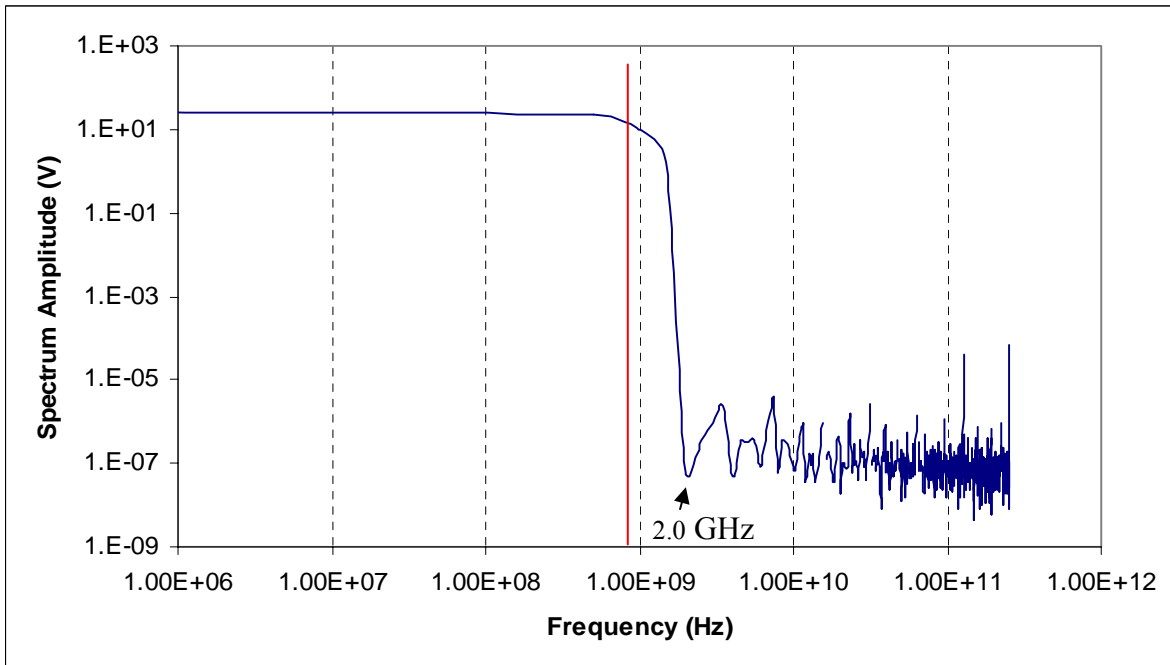


(b) Spectrum

Fig. 2-2 0.75 ns pulse and its spectrum

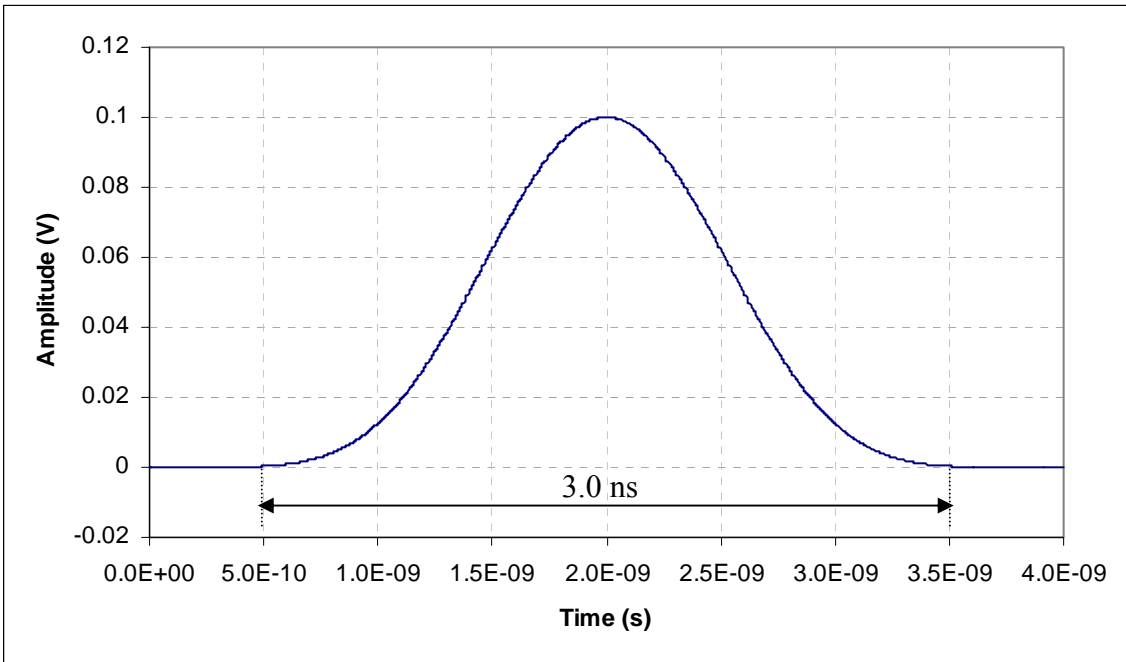


(a) 1.5 ns pulse waveform

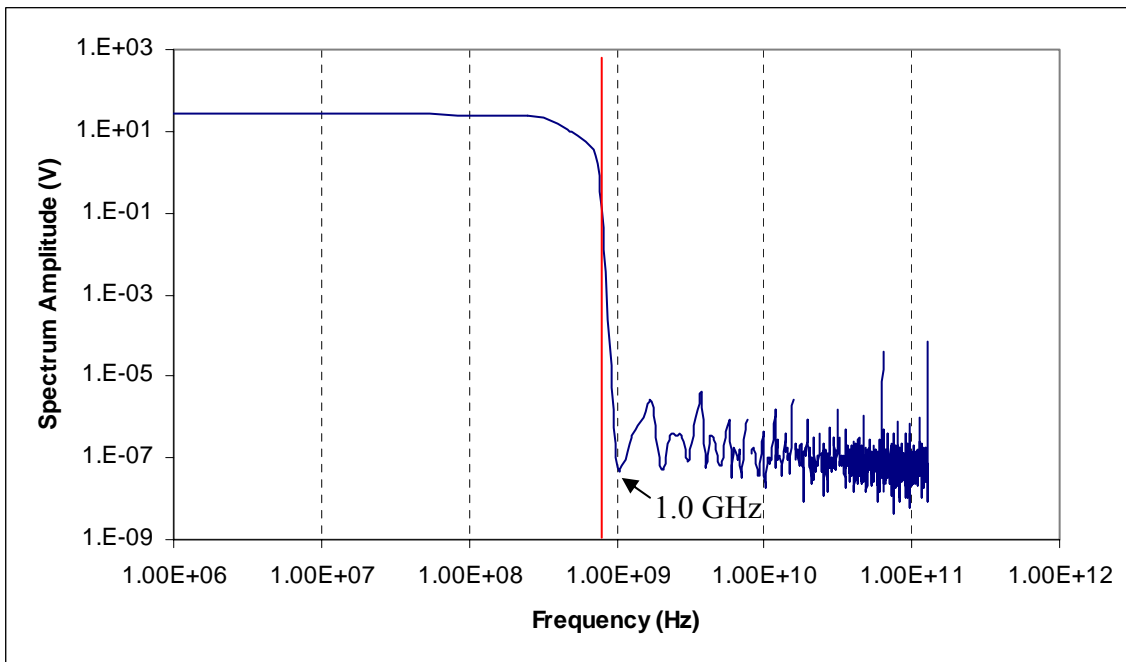


(b) Spectrum

Fig. 2-3 1.5 ns pulse and its spectrum

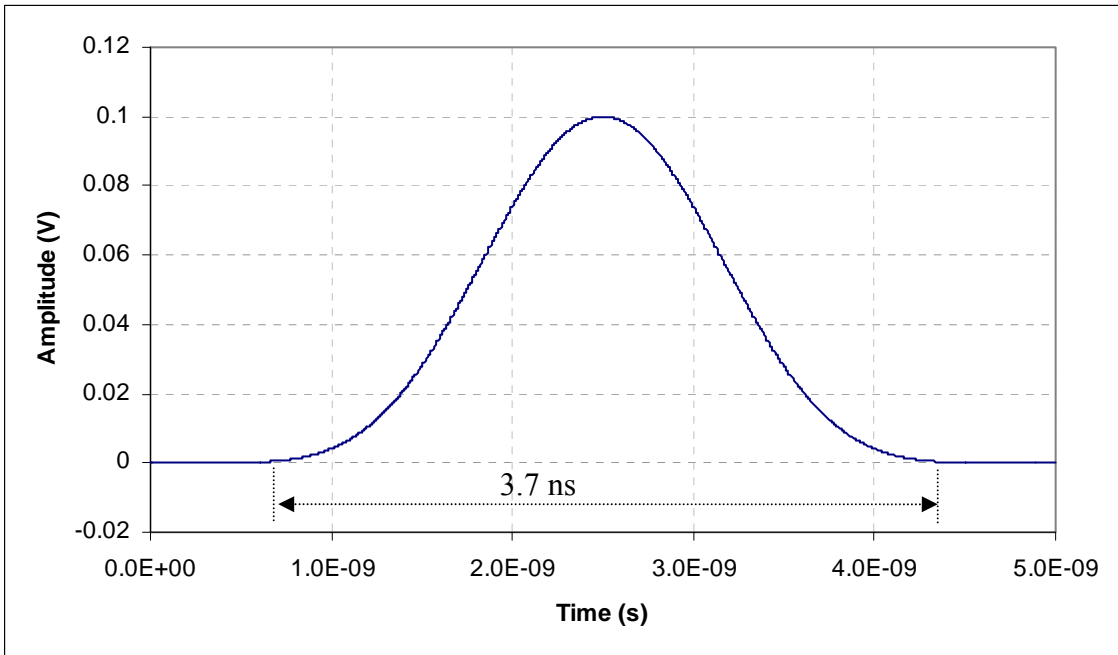


(a) 3 ns pulse waveform

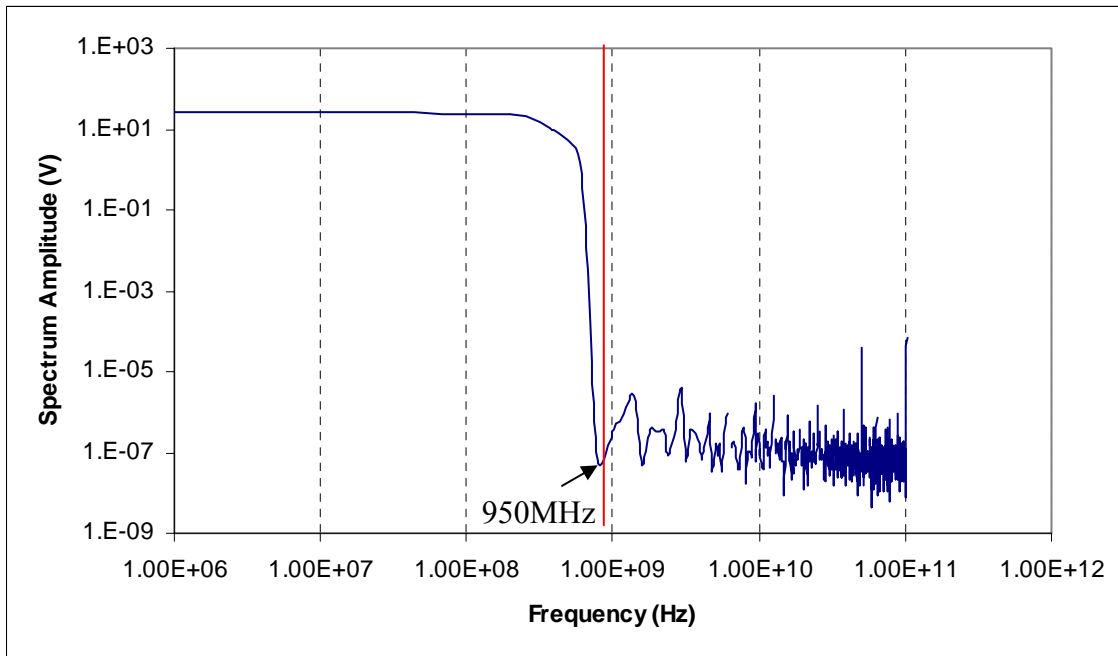


(b) spectrum

Fig. 2-4 3 ns pulse and its spectrum

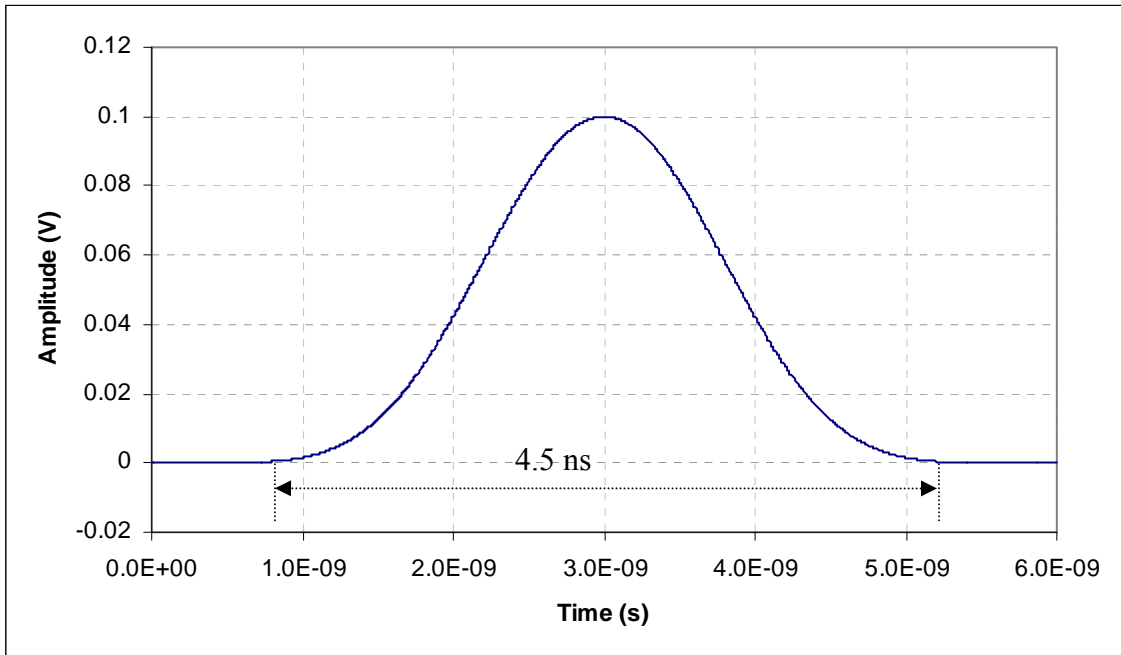


(b) 3.7 ns pulse waveform

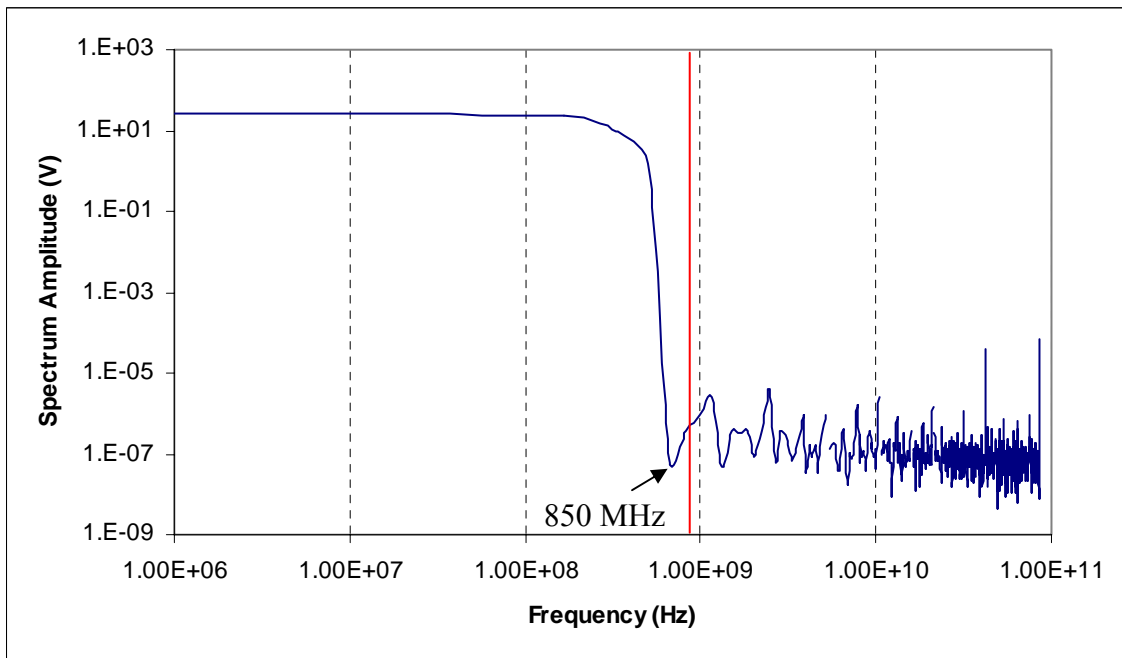


(b) Spectrum

Fig. 2-5 3.7 ns pulse and its spectrum



(b) 4.5 ns pulse waveform



(b) Spectrum

Fig. 2-6 4.5 ns pulse and its spectrum

Even when the pulse width increases to 1.5 ns, as the one in Fig. 2-3, the spectrum still extends to 2 GHz. When the pulse width reaches 3 ns, as shown in Fig. 2-4, the spectrum decreases to 1 GHz. Until the pulse width approaches 3.7 ns, the spectrum finally goes down to 960 MHz, still not reaching the safe region. For a 4.5 ns pulse wave its spectrum contracts to below 850 MHz. Fig. 2-7 summarizes the frequency band of a pulse wave versus its pulse duration.

The above discussions are based on smooth Gaussian type pulses. If a pulse wave has a steeper rising or decreasing edge, it should produce higher frequency components. Hence, 4 ns or wider pulse waves should be chosen for the FCC compliant low frequency GPR. Furthermore, a low pass filter should also be added to prevent unexpected high frequency components.

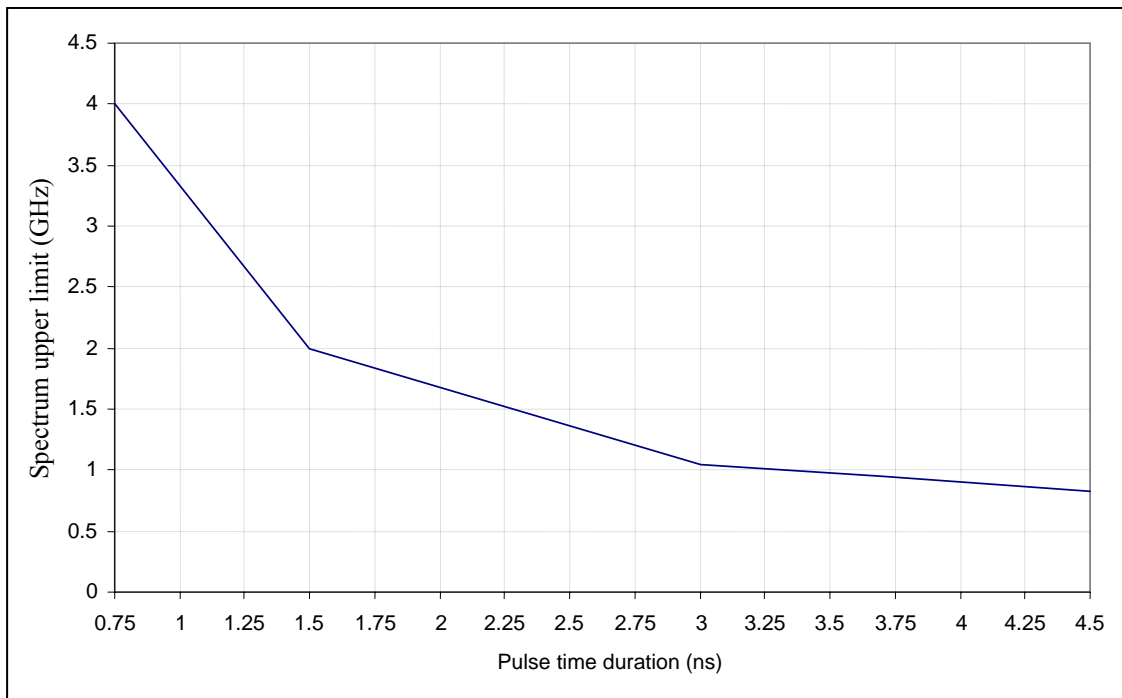


Fig. 2-7 Frequency range of a pulse wave versus pulse time duration

According to the derived pulse widths, new transmitters with satisfactory band range have been developed and integrated into the GPR system. Fig. 2-8 shows the vehicle-mounted ground-coupled pulse GPR developed.



Fig. 2-8 Ground-coupled version of the pulse GPR

2.3 High Frequency GPR

The high frequency GPR is based on frequency-modulated continuous-wave (FMCW) format. The FMCW GPR is composed of a voltage-controlled sweeping transmitter, two ultra-wide-band transmitting and receiving antennas, a receiver, and a host computer for data acquisition and system control, as shown in [Fig. 2-9](#).

The transmitter sends a microwave signal to the pavement and the receiver receives the signal reflected from different pavement layers. The receiver is synchronized with the transmitter. Signals reflected from the pavement are received and processed by the analog and digital circuits. The computer acquires output of the circuits and processes the data, converting it into electrical properties and thickness of the pavement layers. The device developed using FMCW concept is shown in [Fig. 2-10](#).

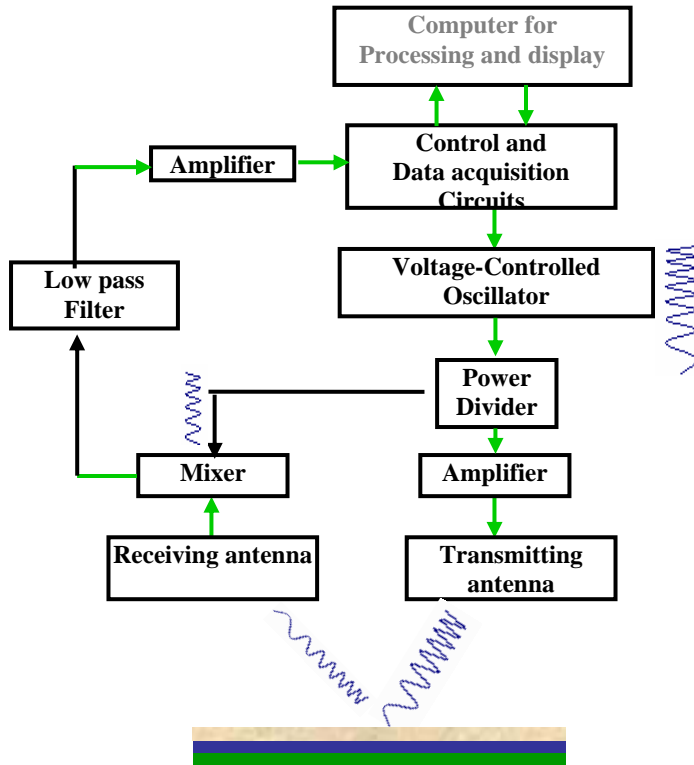


Fig. 2-9 Block diagram of the FMCW radar

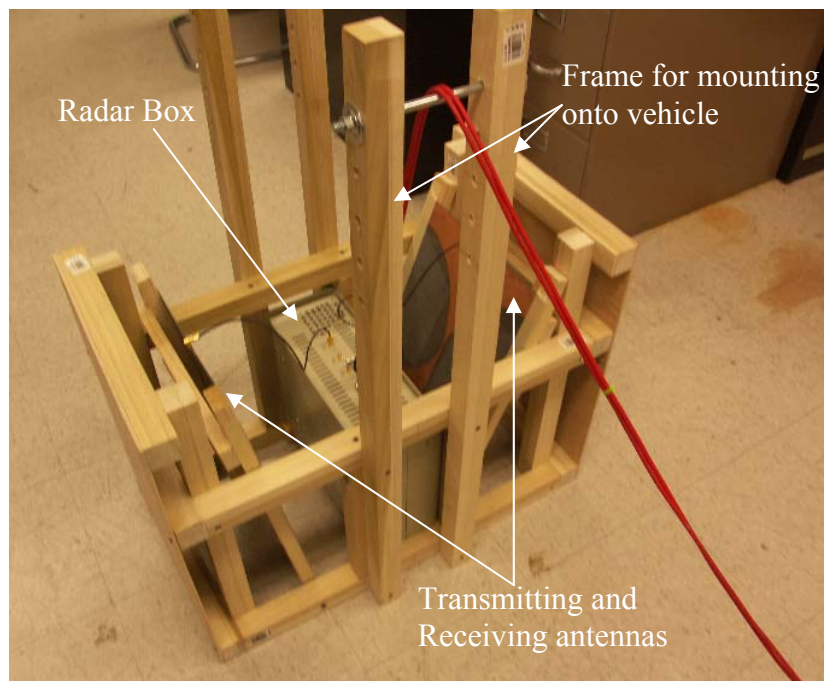


Fig. 2-10 The FMCW system used for measuring properties of pavement layers

2.4 Frequency Control for FMCW GPR

In the FMCW system, the output frequency is controlled by a tuned DC voltage. Usually the output frequency increases with the increase of the tune voltage. Fig. 2-11 shows the measured relationship between the tune voltage and the output frequency of the developed FMCW GPR.

From Fig. 2-11 we see that if the applied tune voltage is above 1.6 DCV, the output frequency of the transmitter will always be above 3.1 GHz, no conflict with FCC regulations. However, the microwave transmitter may have multiple modes being excited; therefore, high pass filters should be employed to cut off the possible frequency components below 3.1 GHz.

Hence, both the pulse GPR and FMCW GPR can be controlled to stay away from the FCC banned frequency range.

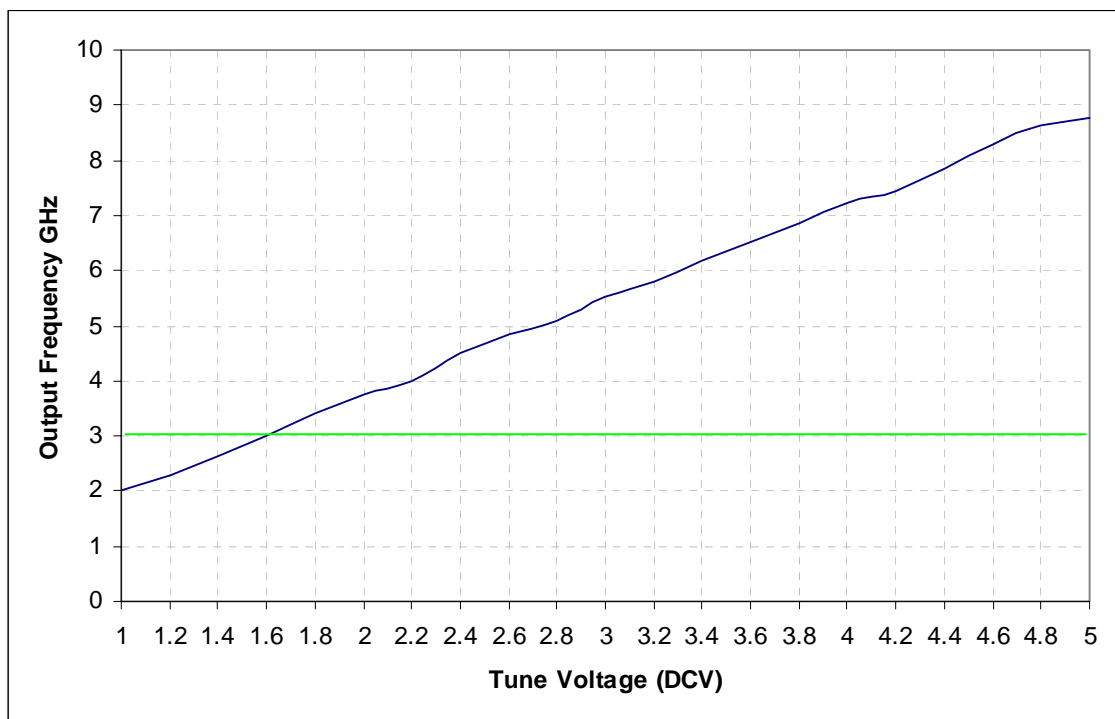


Fig. 2-11 Transmitter's output frequency versus applied tune DC voltage

2.5 Distance Measurement Instrument (DMI) and Global Positioning System (GPS)

A vehicle mounted version of the GPR allowed a faster data production rate but it also brought out a new challenge in the form of distance measurement. The encoder used on the pushcart was not rugged and fast enough to measure distance/speed of the vehicle traveling at 30 miles/hr or more. Thankfully, the vehicle acquired from the Texas Department of Transportation (TxDOT) has a distance measurement device and a GPS system preinstalled in it. In order to utilize this equipment, further study was done to understand the communication protocol used by them to transfer data to the computer. As shown in [Fig. 2-12](#), the DMI/GPS is connected to a data acquisition box. The data acquisition box consists of an input/output (I/O) module and a biscuit PC with a serial port and one Ethernet port. The data acquisition box is connected to a router. The computer is also connected to the router. The data acquisition box is programmed so that it broadcasts the incoming data from the DMI or GPS 4 times/sec over the Ethernet port. [Fig. 2-13](#) shows the equipment setup inside the vehicle.

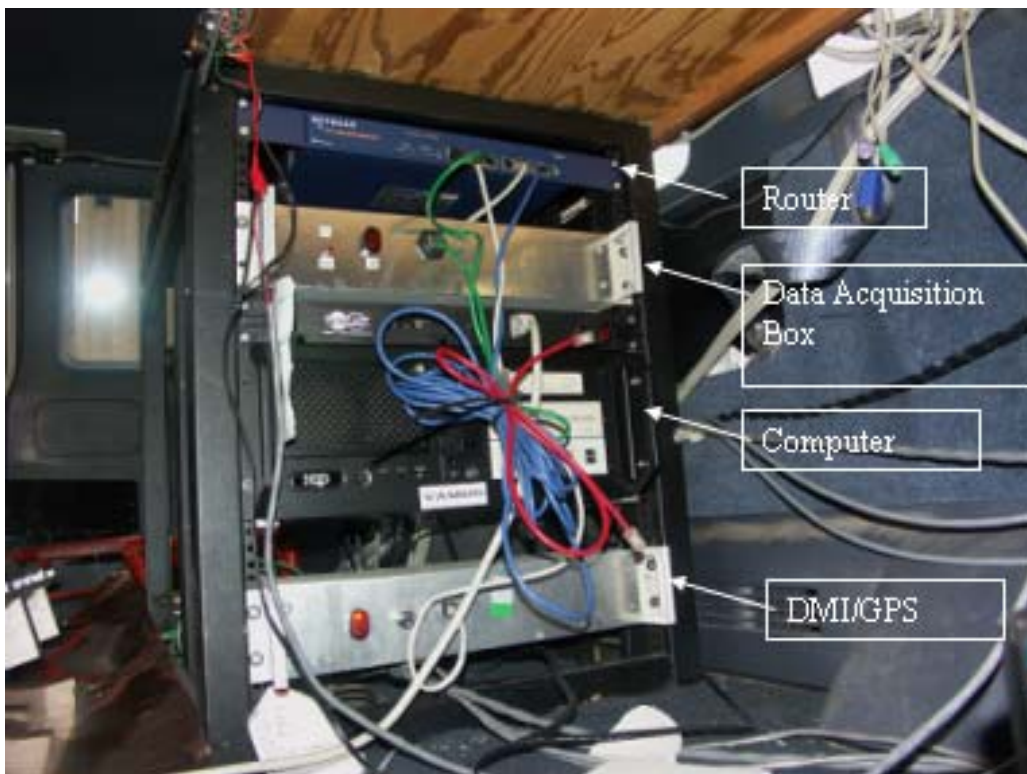


Fig. 2-12 DMI and GPS equipment setup

The whole system uses User Datagram Protocol (UDP) for communication. UDP is often referred to as a connectionless network protocol because it does not form a continuous link between the server and the client. The data are broadcasted in the form of fixed size datagram or packets. This ensures faster data transfer but is also error prone, since often data packets are received out of order or are lost. However, in order to comply with the protocol used by the TxDOT vehicle, UDP was used for communication.

Integrating DMI and GPS data into measured pavement property data would be a great help for the future study and pavement history observation.

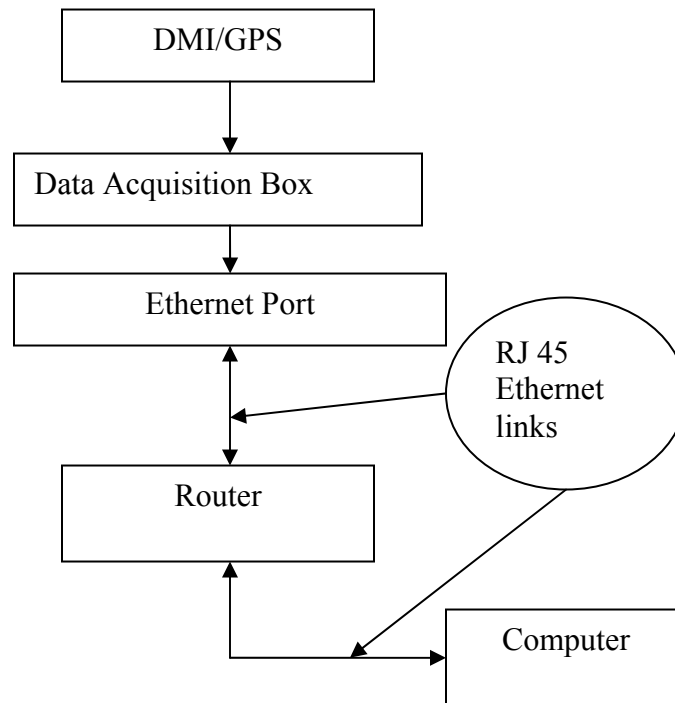


Fig. 2-13 DMI/GPS setup

CHAPTER 3: IMPROVEMENTS IN ALGORITHMS

This chapter will first introduce a new algorithm for estimating pavement dielectric constant directly from ground-coupled GPR data.

3.1 Current Methods for Dielectric Constant Estimation

When using GPR to measure pavement thickness, we have to measure dielectric constant simultaneously. In air-coupled mode, the dielectric constants of pavement materials are usually measured by the surface reflectivity method. At the interface of two mediums, under the condition of normal incidence, the reflection coefficient can be expressed as

$$\Gamma^{surface} = \frac{\sqrt{\varepsilon_2} - \sqrt{\varepsilon_1}}{\sqrt{\varepsilon_2} + \sqrt{\varepsilon_1}} = \frac{V_{ref}^{Surface}}{V_{in}} \quad (3-1)$$

When a metal plate (which can be assumed to be a perfectly conducting surface) is placed on the interface for calibration

$$\Gamma^{metal} = \frac{V_{ref}^{metal}}{V_{in}} = -1 \quad (3-2)$$

In pavement measurements, the medium above the pavement is air and its dielectric constant is 1. Combining Equation (3-1) with Equation (3-2), we obtain:

$$\varepsilon_2 = \left(-\frac{\Gamma^{surface} + 1}{\Gamma^{surface} - 1} \right)^2, \text{ where } \Gamma^{surface} = \frac{V_{ref}^{Surface}}{-V_{ref}^{metal}} \quad (3-3)$$

Using Equation (3-3) to determine pavement dielectric constant is referred to as the surface reflection coefficient method and it only applies to air-coupled GPR.

For ground-coupled GPR, the common middle point (CMP) method and its improved versions [6] are applicable. But the CMP method is based on solving a set of related equations, like Equation (3-4), to obtain the dielectric constant and the pavement depth simultaneously,

$$\left\{ \begin{array}{l} 2\sqrt{\varepsilon_{r1}(x_1^2 + d^2)} - 2x_1 = c \Delta t_1 \\ \min\left(2\sqrt{\varepsilon_{r1}(x_1^2 + d^2)} + 2|l_1 - x_1|\right) \\ \vdots \\ 2\sqrt{\varepsilon_{r1}(x_i^2 + d^2)} - 2x_i = c \Delta t_i \\ \min\left(2\sqrt{\varepsilon_{r1}(x_i^2 + d^2)} + 2|l_i - x_i|\right) \\ \vdots \\ 2\sqrt{\varepsilon_{r1}(x_n^2 + d^2)} - 2x_n = c \Delta t_n \\ \min\left(2\sqrt{\varepsilon_{r1}(x_n^2 + d^2)} + 2|l_n - x_n|\right) \end{array} \right. \quad (3-4)$$

where the subscripts $1, 2, \dots, i, \dots, n$ represent the number of measurements carried out with a bistatic radar over flat layered media, and Δt_i is the time delay of the reflected wave with respect to the direct wave (propagation from the transmitter directly to the receiver through air) in the i th measurement.

But this method is time consuming and not suitable for real time applications. The following section will introduce a new fast method for finding pavement dielectric constant from ground-coupled GPR data.

3.2 New Method for Dielectric Constant Estimation for Ground-Coupled GPR

For ground-coupled GPR, the reflection wave and the direct wave arrive at the same time such that the amplitude of the surface reflection cannot be determined. Hence, the surface reflection method does not apply to ground-coupled GPR. The CMP method does work for ground-coupled GPR, but it is time consuming and not suitable for real time measurements. In this case, we have to search for new methodologies. Fortunately, in our experiments, we observed that a signal always comes immediately after the direct wave as shown in the red dashed circle in Fig. 3-1. Does this signal bring some kind of information that can be used to find the pavement dielectric property? Theoretically, there should be three main wave paths for the ground-coupled GPR shown in Fig. 3-2, where path 1 denotes the direct wave, path 2 represents the layer bottom reflection, and path 3 is a possible ground surface wave path. If the signal shown in the red dashed circle in Fig. 3-1 does propagate along path 3, it surely contains information of pavement dielectric constant. In order to verify the existence of path 3 in real GPR

application cases and to search for new methods for dielectric constant estimation, numerical simulations of ground-coupled GPR are conducted using the Transmission line matrix (TLM method). Fig. 3-3 illustrates the geometry of the GPR setup. The transmitter is at a fixed position, and the receiver is placed at 20, 30, 40, 50, and 60 cm away, respectively, from the transmitter. The simulated waveforms in different transmitter-receiver offsets are given in Fig. 3-4.

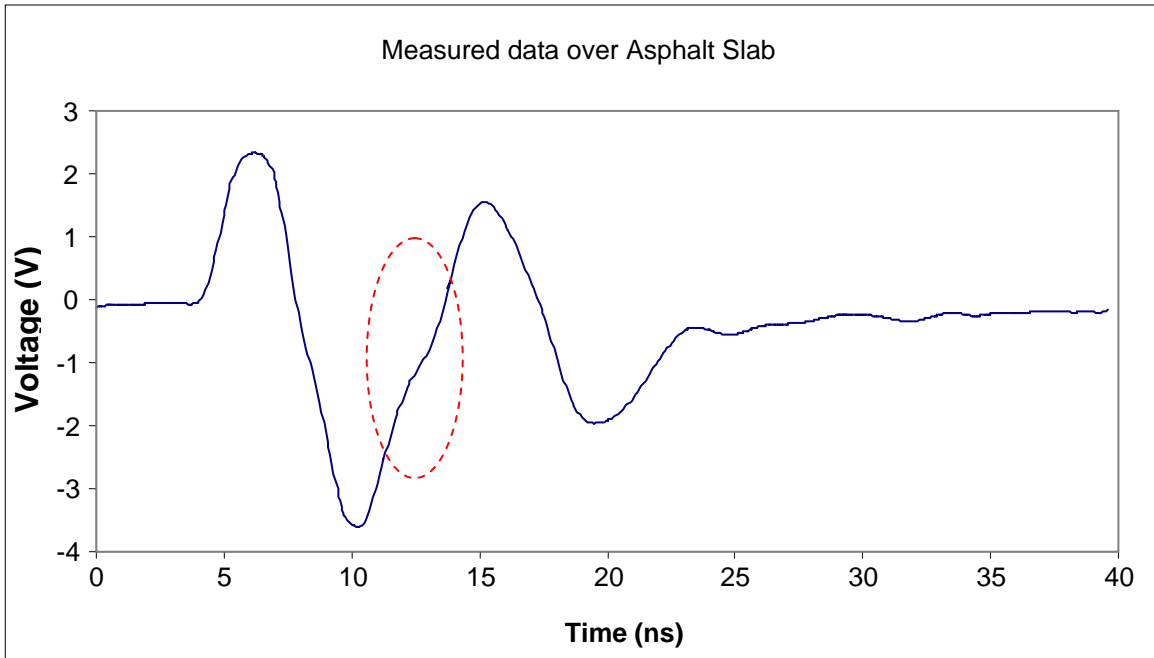


Fig. 3-1 Typical measured ground-coupled GPR waveform

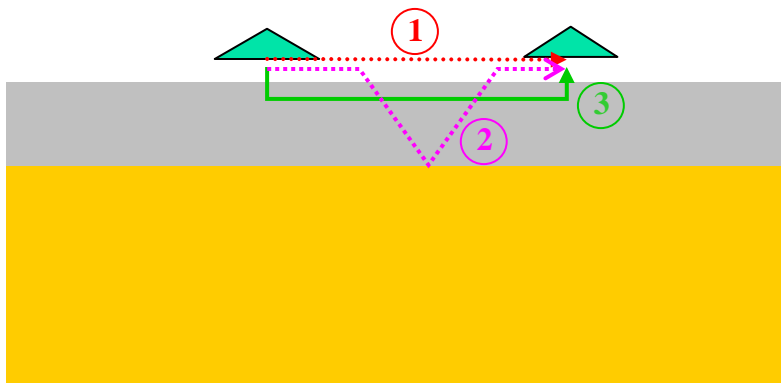


Fig. 3-2 Main wave paths for ground ground-coupled GPR

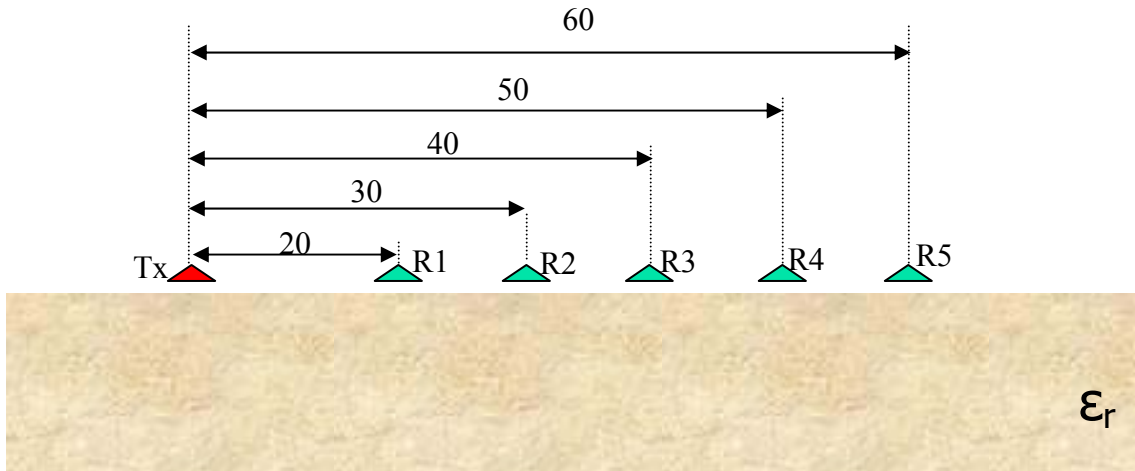


Fig. 3-3 Geometry for numerical simulation

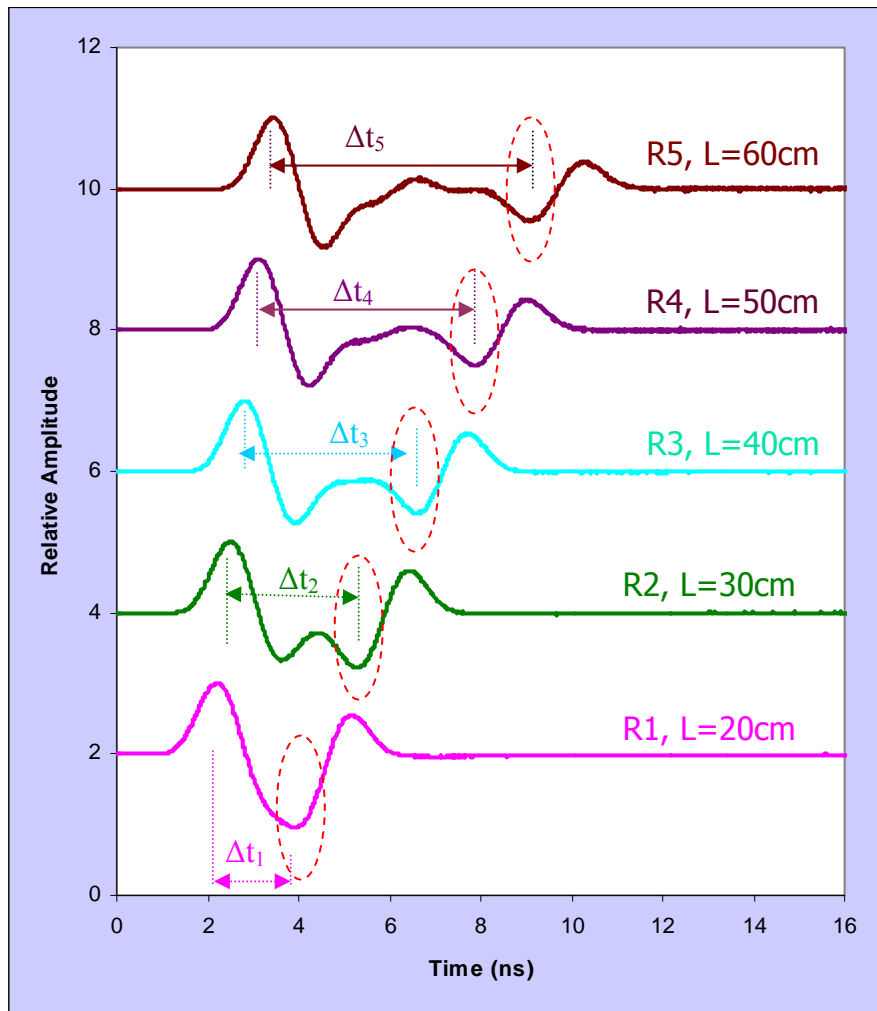


Fig. 3-4 Simulated waveforms at positions R1, R2, R3, R4, and R5

Fig. 3-4 illustrates that the signals in the red dashed circles delay with respect to the direct wave as the transmitter-receiver offset increases. The correspondence of the time delay to the transmitter-receiver offset is plotted in Fig. 3-5, as a blue line. On the other hand, if we assume the wave takes path 3 in Fig. 3-2 and estimate the time delay Δt by,

$$\Delta t = (\sqrt{\varepsilon_r} - 1)L/c \quad (3-5)$$

where L is the transmitter-receiver offset and c is the velocity of light in free space, then it is found that the estimated time delay, see the pink line in Fig. 3-5, is identical to the TLM simulated time delay. This phenomenon implies that the signals in the red circles in Fig. 3-1 and Fig. 3-4 are indeed induced by the pavement. This pavement induced wave is referred to as the ground surface wave. By measuring the time delay of the ground surface wave with respect to the direct wave, the dielectric constant of the pavement can be determined,

$$\varepsilon_r = \left(\frac{c \Delta t}{L} + 1 \right)^2 \quad (3-6)$$

With the dielectric constant predetermined, the thickness of the pavement can be directly solved by analytic formula, and no more iteration is needed. This procedure greatly increases the in-situ processing time, realizing real time measurements.

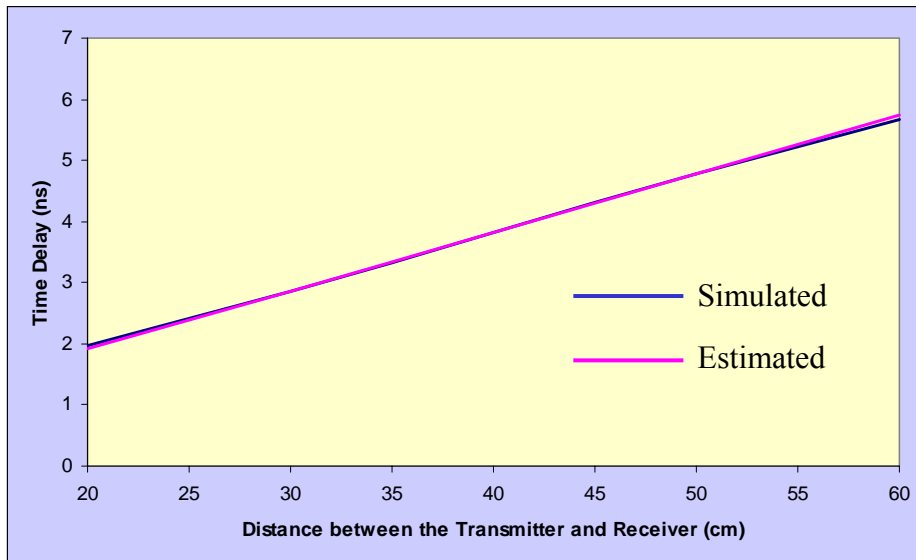


Fig. 3-5 Comparison of simulated time and modeled time

CHAPTER 4: LAB AND FIELD TESTS

In order to evaluate the properties of the developed FCC compliant GPR system, a series of lab and field tests were conducted.

4.1 Lab Tests of FMCW Radar

Figs. 4-1 and 4-2 show the slab and its size used in lab tests. When FMCW radar was set up 13 inches above the asphalt slab, the surface and the bottom reflections were clearly observed, as shown in Fig. 4-3.



Fig. 4-1 Asphalt slabs for lab experiment

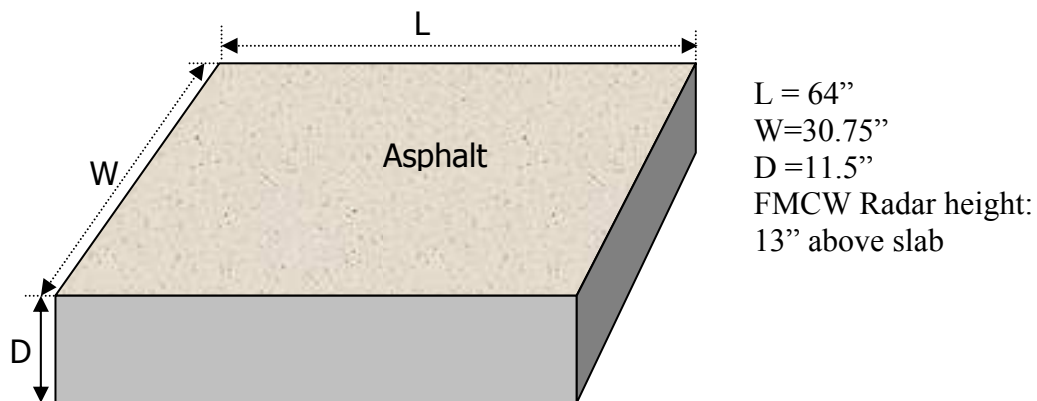


Fig. 4-2 Slab size

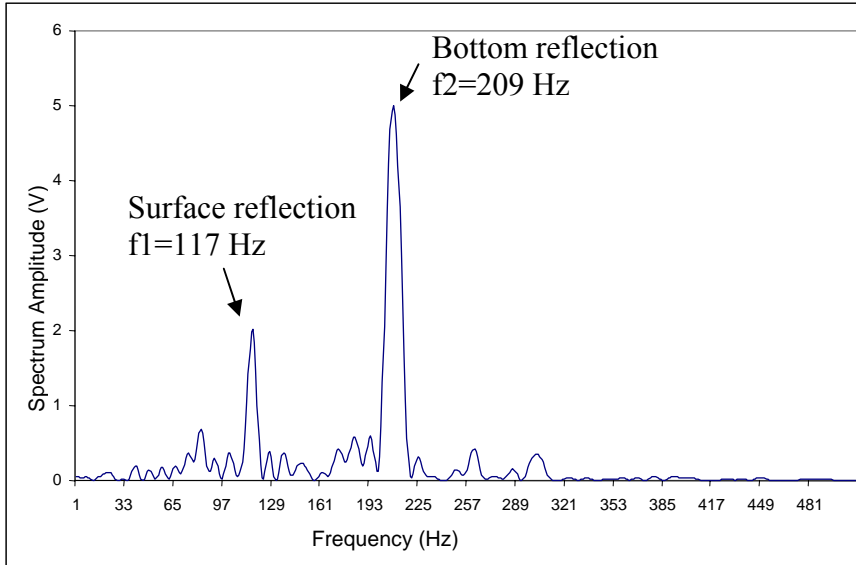


Fig. 4-3 Measured signals on 11.5 inch slab by FMCW GPR

According to the formulas in Equation (4-3) as well as in [6], the dielectric constant of the asphalt slab and the thickness can be calculated by,

$$\epsilon_r = \left[\frac{1+0.3856}{1-0.3856} \right]^2 = 5.086$$

Estimated Thickness:

$$D = 0.04764(f_2 - f_1) \times \frac{30}{2 \times 2.54 \times \sqrt{5.08}}$$

$$= 11.48(\text{inch})$$

The FMCW-measured thickness of 11.48 inches is very close to the real slab thickness of 11.5 inches. It proves that the developed FMCW radar is working properly. To further investigate the performance of this radar, a test over a parking lot pavement was also carried out. The real thickness in the parking lot is 2.75 inches, as shown in Fig. 4-4. One of the measured waveforms is given in Fig. 4-5 and the eight measured thickness at eight positions near the cutting edge are given in Table 4-1.

Table 4-1 Measured thickness of a parking lot pavement

Meas. Points	1	2	3	4	5	6	7	8
Calculated Depth (inch)	2.650	2.743	2.740	2.686	2.746	2.825	2.8790	2.794



Fig. 4-4 A parking lot asphalt pavement with a thickness around 2.75 inches

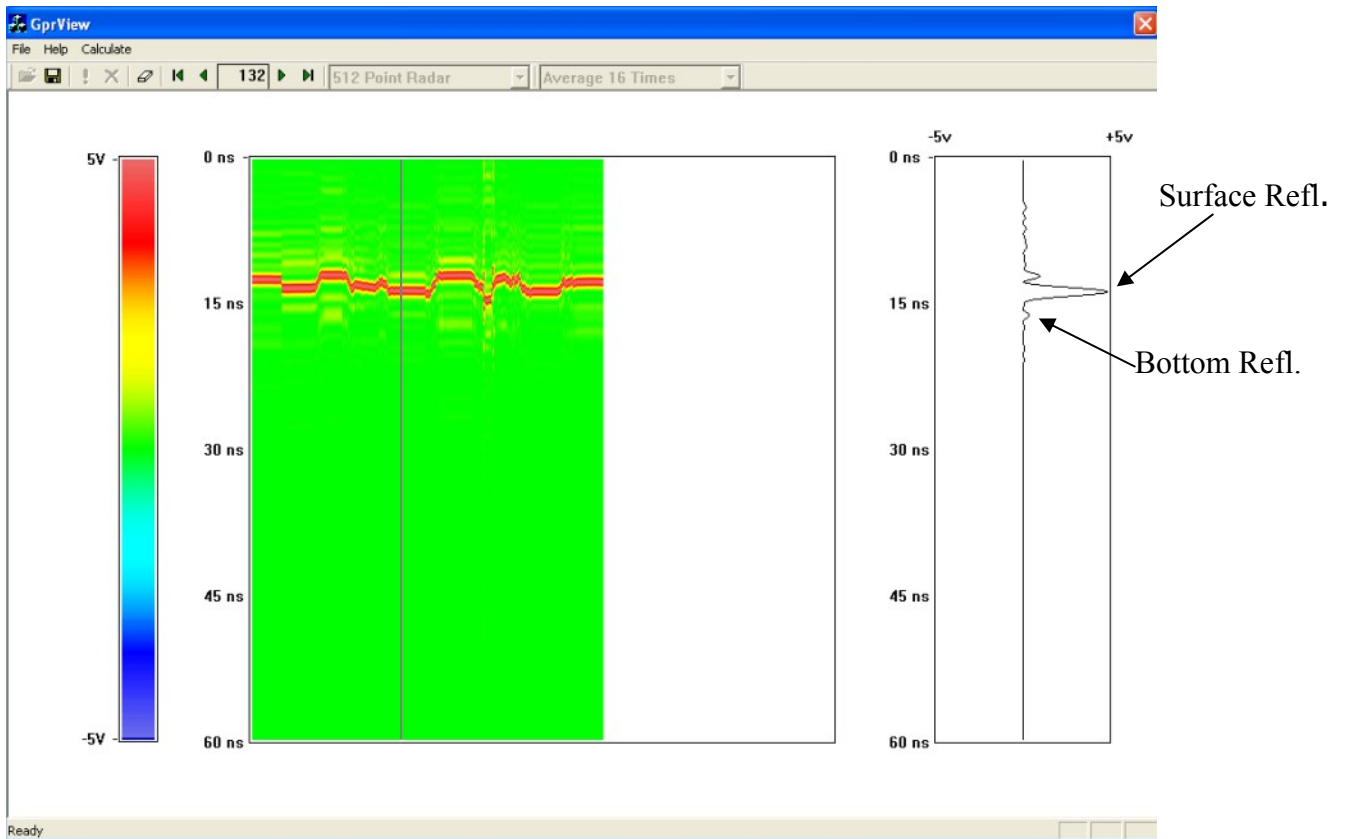


Fig. 4-5 Measured FMCW radar waveform over the parking lot

The results in [Table 4-1](#) demonstrate very good agreement between the FMCW-measured results and the ruler-measured ones.

Comparing the pavement bottom reflection amplitudes in [Fig. 4-3](#) and [Fig. 4-5](#), one can easily notice that the slab bottom reflects a very strong signal and the parking lot pavement sends back a very weak reflection. Obviously, it is not caused by the attenuation along the traveling paths in asphalt material, because the slab is much thicker than the pavement and should have a much longer path. The only cause is the reflection coefficient at the bottom interface that is determined by the dielectric constant contrast between the pavement asphalt and the material under the pavement. As we know, the bigger the dielectrics' contrast across the interface, the larger the reflection coefficient at the interface. The slab in the lab is set up a few centimeters above the floor; hence, the bottom interface of the slab is between air and asphalt and the dielectric contrast is about 5:1. While in the parking lot, the bottom interface of the pavement is between asphalt and the base soil; the dielectric contrast there is about 5:4, much closer than that of asphalt to air contrast. Therefore, the slab bottom interface reflects a much stronger signal. This phenomenon implies that if the dielectric constant of a pavement is too close to that of the material under the pavement, FMCW radar may suffer difficulty in identifying the reflection signals of the pavement layers.

4.2 Lab Tests of Pulse GPR

The frequencies used by the pulse GPR are pretty low; hence, the waveforms of pulse GPR are relatively smooth, which causes difficulties in accurate travel time estimation. To solve this problem, a metal plate calibration technique is employed to cancel the effect of direct waves. The yellow line in [Fig. 4-6](#) is the metal-calibrated reflection signal of the pulse GPR measurement over the slab shown in [Fig. 4-1](#). Based on the reflection peak on the yellow line, the travel time of the slab bottom interface reflection is easily read out.

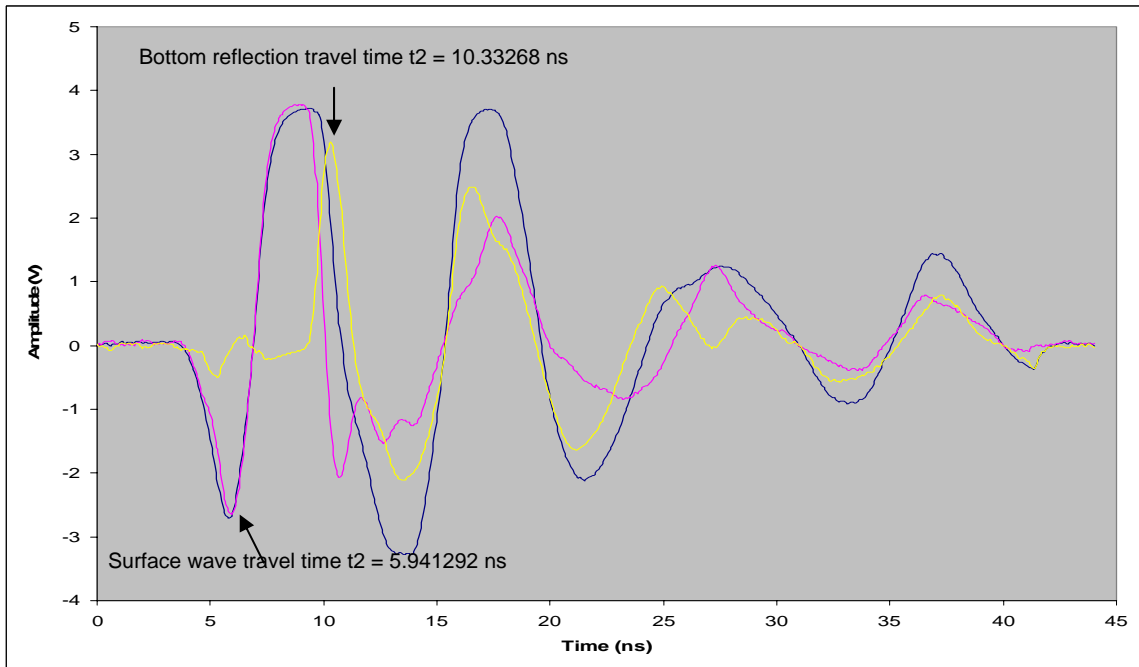


Fig. 4-6 Waveforms measured by pulse GPR over the asphalt slab

$$\begin{aligned}
 D^{PulseGPR} &= \frac{30 \times (t_1 - t_2)}{2 \times 2.54 \times \sqrt{5.085}} \\
 &= 11.49 \text{ inches}
 \end{aligned}$$

This result is very close to the real thickness.

4.3 Field Tests

The first GPR field test was carried out at the Texas Transportation Institute (TTI) Annex. The pavement is over 2000 feet long with the distance marks on side. The measurement started from the mark “-200” and ended at mark “1810,” a total of 2010 feet of pavement was measured. The result measured by ground-coupled GPR is given in [Fig. 4-7](#).

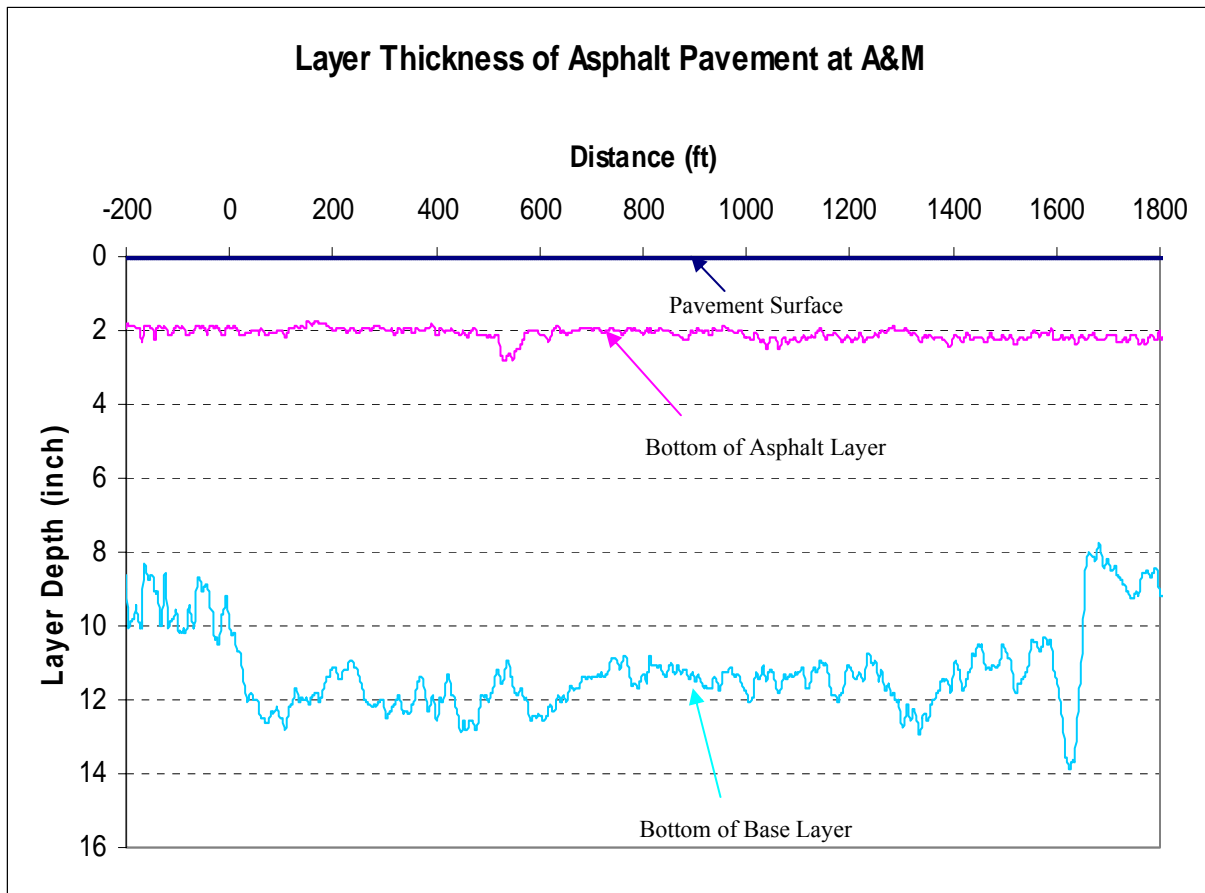


Fig. 4-7 Measured over the TTI Annex by ground ground-coupled GPR

According to the GPR data, two layers of pavement are detected, as shown in Fig. 4-7. The first layer, an asphalt layer, has a thickness around 2 inches from the mark “0” to “1810”; while its thickness varies from 2 to 4 inches at the locations from mark “-200” to mark “0.” The second layer has an average depth around 12 inches from mark “-200” to mark “1590”; about 3 to 4 inches shallower near the two ends of the pavement; the deepest section of the second layer is located between the mark “1590” to “1650,” about 14 inches. Fig. 4-8 is measured by pulse ground-coupled GPR on SH21. It is very close to that measured by TxDOT radar.



Fig. 4-8 Measured result on SH21 in Bryan

CHAPTER 5: CONCLUSIONS AND RECOMMENDATIONS

5.1 Conclusions

In this project, a hybrid GPR system has been successfully developed. This system is composed of two sub-systems, a low frequency pulse GPR and a high frequency FMCW GPR. At this time, both the FMCW GPR and pulse GPR are vehicle mounted. New software has been composed to cooperate with the vehicle DMI device. The software for signal processing and format setting has also been improved for real time display, and no post-processing is required. The GPR data format is now compatible with TxDOT software, which benefits information sharing and the implementation of this FCC compliant GPR system.

Lab tests and field tests have been conducted. The measured results agreed with the real cases very well.

5.2 Recommendations

The developed GPR system is able to collect pavement layer information accurately. An air-coupled version of pulse GPR would be much more attractive in applications, because it is easier to operate and can work at highway speed.

REFERENCES

- [1] A. Loulizi, *Development of Ground Penetrating Radar Signal Modeling and Implementation For Transportation Infrastructure Assessment*, Virginia Polytechnic Institute and State University, Feb 2001.
- [2] S. Lahour, *Development of Data Analysis Algorithms for Interpretation of Ground Penetrating Radar Data*, Virginia Polytechnic Institute and State University, Oct 2003.
- [3] A. P. Annan, *GPR Principles Procedures & Applications*, Sensors & Software Inc., Canada, 2003.
- [4] http://fate.clu-in.org/gpr_main.asp
- [5] <http://www.lpi.usra.edu/meetings/lpsc2004/pdf/1563.pdf>
- [6] Liu, C., Li, J., Gan, X., Xing, H. and Chen, X. "New Model for Estimating the Thickness and Permittivity of Subsurface Layers from GPR Data," *IEE Proc. – Radar, Sonar and Navigation*, Vol. 149, No. 6, pp. 315-319, December 2002.

